Photoluminescence of disorder-induced localized states in $GaAs/Al_xGa_{1-x}As$ superlattices

L. Pavesi, E. Tuncel, B. Zimmermann, and F. K. Reinhart
Institut de Micro- et Optoélectronique, Ecole Polytechnique Fédérale de Lausanne, CH-1015 Lausanne, Switzerland
(Received 11 July 1988; revised manuscript received 23 November 1988)

Purposely disordered $GaAs/Al_xGa_{1-x}As$ superlattices, followed by an enlarged well, were grown by molecular-beam epitaxy. Selective-excitation photoluminescence measurements were performed to study the energy dependence of the motion of resonantly photocreated excitons in disordered superlattices. We report the existence of different energy regions in the superlattice bands, corresponding to extended and spatially confined (localized) states induced by disorder. The temperature dependence of the photoluminescence spectra suggests the existence of activation energies for the localized states. This reflects itself by an increase in the propagation rate of excitons by increasing the temperature. We compare qualitatively the experimental findings with a calculation of the superlattice miniband spectrum.

I. INTRODUCTION

The effect of disorder or quasiperiodicity on carrier propagations in quasi-one-dimensional structures is a field of growing interest and has been studied both theoretically[1–3] and experimentally.[4–6] Molecular-beam epitaxy (MBE) grown $GaAs/Al_xGa_{1-x}As$ superlattices (SL) are well suited for the observation of such effects. The monolayer control of the growth sequence permits the fabrication of purposely disordered SL. In these structures the electronic properties in the growth direction (we will call it vertical direction) are governed by the layer sequences. In SL $Al_xGa_{1-x}As$ barriers are thin compared to the penetration length of the well wave functions. Thus, there is coupling between adjacent GaAs wells. Due to the coupling there is formation of energy minibands whose width and position are characteristic of the layer sequence. In the vertical direction of a periodic SL, the electron and hole eigenstates are Bloch-type functions that have the periodicity of the superlattice. Vertical motion of electrons and holes can occur via miniband states.[7] The photoexcited electrons and holes can either move with a different mobility or form excitons.

In the following we study the weak-disorder limit. The disorder is introduced as random, small variations of the well thicknesses around a mean value. In this limit we can still discuss our results in the framework of the envelope function approximation. Randomizing the layer sequence widens the SL minibands and sometimes introduces splittings within a given miniband (subband and minigap formation). At the miniband extrema appear localized states.

Excitons whose eigenstates belong to extended states can propagate, whereas those from localized states undergo three regimes of propagation as a function of temperature. At very low temperatures, they are spatially trapped and cannot move. At intermediate temperatures, excitons may move between different wells via phonon-assisted transitions and the consequent propagation is called variable range hopping.[8] At higher temperatures, excitons are excited into extended states, and excitonic diffusion takes place.[9]

In this article it is our purpose to report some experimental evidence on the existence of regions of localized and extended states in the miniband structure of a purposely disordered SL. We have studied these systems by using variable temperature selective excitation photoluminescence (SEPL). With this technique we control the energy range in which carriers are created by selecting the energy of the exciting light, $\hbar\omega_x$. By scanning $\hbar\omega_x$ through the electron-heavy-hole (e-hh) exciton emission band of the superlattice, we can choose the spatial character of the states (extended or localized) of the electron and heavy-hole pairs generated. An enlarged well (EW) grown below the superlattice acts as a sink for the excited carriers.[5] The observed fluctuations in the emission intensity of the EW reflect photogeneration of alternatively mobile and localized carriers. This perpendicular motion of electrons and holes has already been evidenced by photoluminescence,[5,6] time-resolved photoluminescence,[7,10] and electrical measurements.[11]

In this article we continue our analysis of disordered SL by qualitatively comparing SEPL spectra and SL miniband calculations. The energy spectrum of the SL is calculated by solving the Schrödinger equation for electrons and heavy holes with the usual boundary conditions[12] by the method of finite elements. We neglected the light holes because we normally worked at low temperatures where these states are mainly empty. We have considered parabolic dispersion in the layer planes, neglected excitonic effects, and used the independent particle approximation. Thus we can only qualitatively describe the experimental results.

We study the PL spectra evolution as a function of the sample temperature. For the excitonic motion in the vertical direction we observe a continuous crossover from variable range hopping transport at low temperatures to diffusive transport via extended states at high temperatures.

II. EXPERIMENTAL SETUP

The measurements were made using a continuous flow cryostat and a double monochromator. The energy resolution was of 0.5 meV. Detection was with a cooled GaAs photomultiplier tube, followed by a photon counting system and a multichannel analyzer. An argon pumped styryl 8 dye laser was used to excite the SEPL. The wavelength of the laser light was chosen to excite resonantly the SL excitons. The laser beam was focused to a diameter of about 50 μm and to a power density of about 130 mW/cm^2. The layers were excited homogeneously because the pumping light penetrates to depths of the order of 3–4 μm whereas the total thickness of the SL was about 0.3 μm. Lateral homogeneity of the layers was checked by repeating measurements on different spots of each sample.

The samples used were grown in a 360 Varian MBE machine, on n-type GaAs substrates.[13] The growth sequence was the following: (i) buffer layer—GaAs 500 Å, AlAs 100 Å, GaAs 4000 Å, and a superlattice $Al_xGa_{1-x}As$ 30 Å, GaAs 30 Å (49 periods); (ii) EW—GaAs 60 Å, acts as the trapping site; (iii) superlattice SL (49 periods)—differs from one sample to another. The aluminum content was always taken to be 35%. In sample A, SL is ordered and consists of 49 periods of $Al_xGa_{1-x}As$ 30 Å, GaAs 30 Å. In sample B, well thicknesses in SL are random variables with a discrete Gaussian distribution (mean well width of 30 Å, standard deviation of 6 Å). The actual sequence used is given in Table I.

TABLE I. Well sequence used to grow the disordered superlattice. The column labeled No. numerates the well sequence starting from the enlarged well side. The discrete Gaussian distribution was constructed by taking values from -3σ to $+3\sigma$ around the mean value. The choice of well widths were taken to insure sufficient aperture times for oven shutters during growth (Ref. 13).

No.	Å	No.	Å	No.	Å	No.	Å	No.	Å
1	35	2	35	3	31	4	31	5	27
6	23	7	31	8	35	9	23	10	35
11	23	12	27	13	31	14	31	15	31
16	27	17	31	18	31	19	11	20	31
21	23	22	31	23	23	24	35	25	35
26	15	27	27	28	31	29	31	30	31
31	27	32	31	33	35	34	39	35	39
36	31	37	23	38	31	39	23	40	27
41	31	42	31	43	39	44	27	45	23
46	39	47	27	48	19	49	31		

III. DISORDER EFFECTS IN SL MINIBANDS

In this section we compute the energy spectrum of two superlattices similar to the ones we have experimentally studied. We have considered only the SL and not the complete system of SL+EW+buffer. We are only interested in disorder effects on the excitonic propagation, disregarding the particulars of excitonic trapping into the EW.[14] We calculate the electron and heavy-hole eigenenergies E and the associated envelope wave functions χ by solving the one-dimensional effective-mass Schrödinger equation over the whole SL

$$-\frac{\hbar^2}{2}\frac{d}{dz}\left[\frac{1}{m^*(z)}\frac{d\chi(z)}{dz}\right]+V(z)\chi(z)=E\chi(z)\ , \quad (1)$$

where z is the growth direction. In Eq. (1), $m^*(z)$ is the effective mass of an electron or heavy hole, respectively, and $V(z)$ is the conduction-band edge or the valence-band edge, respectively. We have used bulk values for the effective masses in the two materials because we are in the weak-disorder limit where the miniband picture is still valid.

We discretize Eq. (1) with a finite element method. The discretization leads us to a matrix eigenvalue problem of the form

$$\mathbf{A}\chi=E\mathbf{B}\chi\ , \quad (2)$$

where $\mathbf{A}$ and $\mathbf{B}$ are real, symmetric matrices. We then calculate the eigenvalues E and the eigenfunctions χ by inverse iteration.[15]

The energy spectra and wave functions obtained with this method[16] are shown in Fig. 1. The ordered case (which simulates sample A) is presented in Fig. 1(a): We can see a single electronic miniband centered at 144 meV above the GaAs conduction-band edge and 54 meV large. There are two heavy-hole minibands: one centered at 37 meV below the GaAs valence-band edge and 2 meV large, the other centered at 133 meV and 20 meV large. The wave functions are extended over the whole SL region both for the electrons and for the heavy holes. They have maxima (minima) in the regions of wells (barriers). The contrast between maxima and minima is stronger for the heavy holes (less penetration in the barrier) due to their higher mass.

In Fig. 1(b) we show the same quantities for a disordered SL. The layer sequence is the same as that used for the growth of sample B. The details of the miniband structure are presented in Fig. 2 and Table II. We see a quite homogeneous broadening of the electronic miniband which has a width of 92 meV (disregarding the isolated higher energy levels) and a mean value of 148 meV. The successive eigenenergies within the electron miniband are separated by about 1–2 meV. We observe a 4-meV-wide minigap at about 150 meV. On the other hand, for the heavy holes, the low-energy miniband splits into subbands, and the high-energy miniband broadens. In particular, the 37-meV miniband splits into five subbands of width less than 2 meV each. They are separated by minigaps large of about 4–6 meV.

In Fig. 2 we show the density of states (DOS) obtained

for this layer sequence (solid line) compared with the DOS of the ordered SL (dashed line). We can see the broadened distribution of states for the first electron miniband, 2(a), and the five steps associated with the split first heavy-hole miniband and the broadened second heavy hole miniband 2(b). We note that the total number of heavy-hole bound states is not equal for the ordered and the disordered SL due to the fact that the disordered SL contains wells which admit only one heavy-hole bound state due to their small thickness.

In Fig. 3 we show some electronic (left part) and heavy-hole (right part) wave functions for the disordered SL. Both the electronic and heavy-hole wave functions are localized in definite spatial regions which can be different for the electron and heavy hole of the same level number n. The electronic wave functions are confined to a region of about six wells for energies at the miniband extrema and on 15–20 wells for energies at the center of the miniband. We call the latter states "extended" as they cover a larger sample region. The heavy-hole wave functions, on the contrary, remain confined to two or

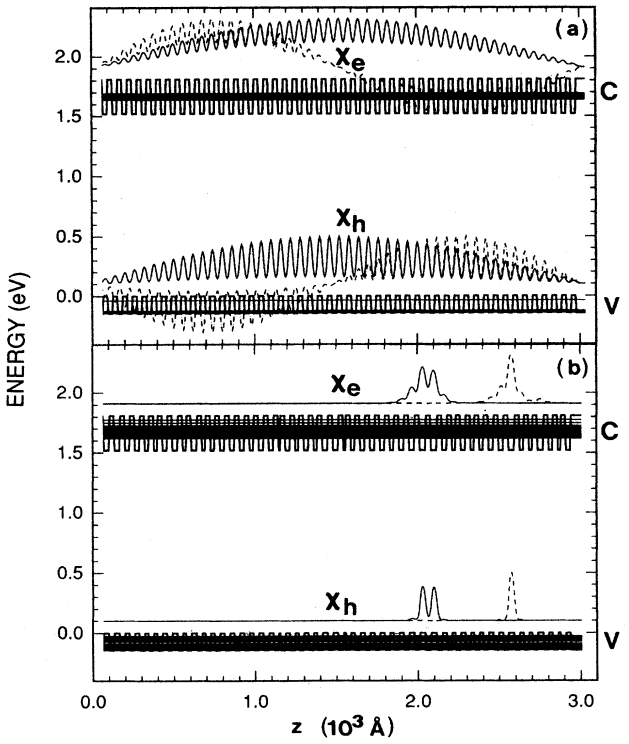

FIG. 1. Valence- (V) and conduction- (C) band variations as a function of the growth coordinate z for an ordered (a) and a disordered (b) superlattice. For the growth sequence, see the text and Table I. Also shown are the superlattice minibands calculated for electrons and heavy holes. The solid and dashed lines are the $n=1$ and $n=2$ envelope wave functions for the electron [$\chi_e(z)$, upper lines] and heavy holes [$\chi_h(z)$, lower lines] shown in arbitrary units. We have normalized the wave functions to unity over the sample length. The zero of the energy scale is taken to be at the top of the GaAs valence band. For the details of the miniband structure see Fig. 2 and Table II.

TABLE II. Parameters of the first heavy-hole split miniband. $\langle E \rangle$ is the mean energy of a subband and Δ is its width. N is the number of eigenenergies belonging to each subband. L_w is the well thickness associated with the subband. E_t is the transition energy computed as specified in the text. Expt. peak is the energy position of the photoluminescence peaks.

$\langle E \rangle$ (meV)	Δ (meV)	N	L_w (Å)	E_t (eV)	Expt. peak (eV)
26.4	1.7	4	39	1.638	
30.6	1.4	7	35	1.648	1.652
36.1	1.1	19	31	1.669	1.670
41.9	0.1	8	27	1.705	1.685
51.0	0.1	8	23	1.745	1.692

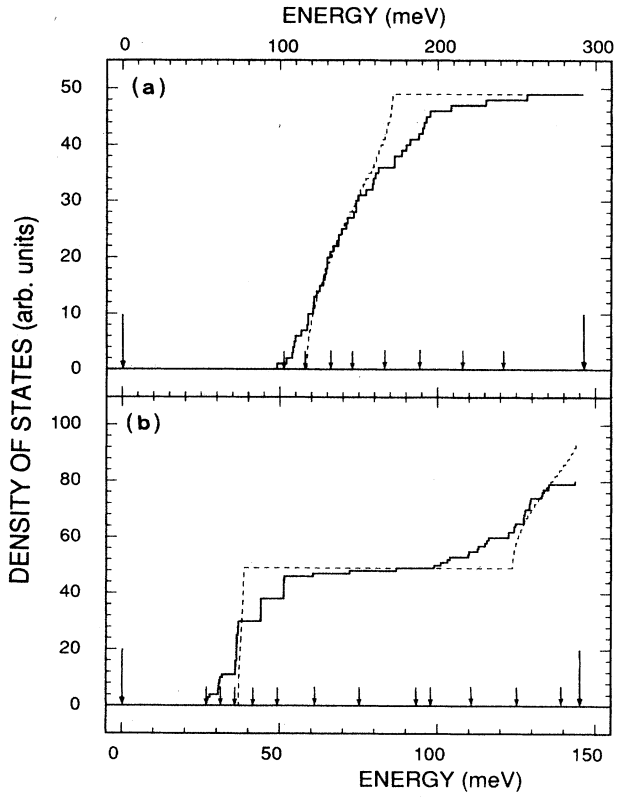

FIG. 2. Density of states (DOS) of the ordered (dashed line) and disordered (solid line) superlattice. (a) The electronic DOS, (b) the heavy-hole DOS. The energy scale is chosen to be zero at the bottom of the conduction band [indicated by a long arrow (a)] and at the top of the valence band [indicated by a long arrow (b)]. The long arrows at high energies mark the energy barriers for electrons and heavy holes (i.e., the bottom of the conduction band and the top of the valence band for the barriers, respectively). The short arrows indicate the eigenenergies for single quantum wells of the following thicknesses: 39, 35, 31, 27, 23, 19, 15, 11 Å. The arrow sequence starts at low energy with the eigenenergy of the widest well and continuous progressively. For the heavy holes, there are two bound states for some wells (namely, 39, 35, 31, 27 Å). The DOS for motion in the parallel direction has been taken as a step function.

three wells whatever the energy in the subbands. The higher effective mass of the heavy holes results in a lower penetration of the wave function into the barriers. Accordingly, the heavy-hole states are more influenced by the local distribution of well thicknesses than the electronic states, which average the local distribution of thicknesses. As a result, the heavy-hole states of the first miniband resemble more the isolated quantum-well states and their associated subbands have a quasiflat dispersion.

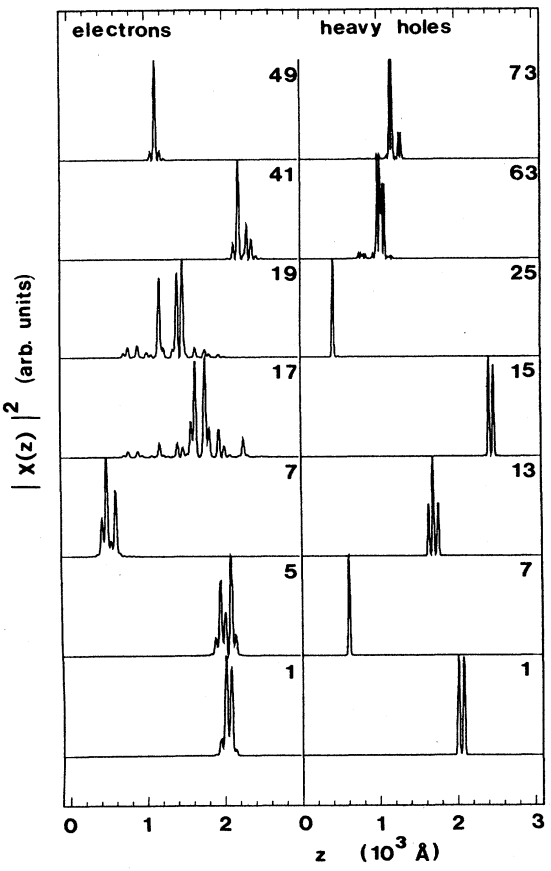

FIG. 3. Probability density $[|\chi(z)|^2]$ to find an electron (left part) or a heavy hole (right part) in the disordered superlattice B. The numbers shown correspond to an index n that we have used to numerate the different eigenenergies of the Schrödinger equation. The eigenenergies of the states shown are the following: (electrons) $n=1$, $E=96.5$, meV; $n=5$, $E=108.7$ meV; $n=7$, $E=113.4$ meV; $n=17$, $E=127.8$ meV; $n=19$, $E=129.3$ meV; $n=41$, $E=181.8$ meV; $n=49$, $E=256.4$ meV; (heavy holes) $n=1$, $E=25.8$ meV; $n=7$, $E=30.4$ meV; $n=13$, $E=35.6$ meV; $n=15$, $E=35.7$ meV; $n=25$, $E=36.1$ meV; $n=63$, $E=124.0$ meV; $n=73$, $E=129.1$ meV. The layer sequence is the same as in Fig. 1(b). The different probability densities are normalized to their maxima. We note that, for the heavy holes, the $n=1$ and $n=7$ states belong to different subbands, whereas the $n=13$, $n=15$, $n=25$ states are of the same subband. The $n=63$ and the $n=73$ states belong to the second heavy-hole miniband. The electronic states are all of the same miniband with the $n=1$ and $n=49$ states at the miniband extrema.

The number of eigenenergies contained in each subband is equal to the number of wells of each thickness in the layer sequence (see Table II). Their energy values correspond to the isolated quantum-well eigenenergy [given by arrows in Fig. 2(b)]. Therefore the subbands are due to resonant coupling of states localized in wells having the same thicknesses as indicated in Table II. Moreover, the heavy-hole envelope wave functions are more confined than the electronic ones so the excitonic propagation properties will reflect the heavy-hole localization.[17]

IV. SELECTIVE ENERGY PHOTOLUMINESCENCE RESULTS

In Fig. 4 we show the photoluminescence spectrum of the ordered sample A. The excitation energy was 1.718 eV. The emission at 1.59 eV is due to the excitonic recombination in the 60-Å well and the emission at 1.67 eV is due to the excitonic recombination in the SL. We show in the inset the calculated energy miniband structure for our sample and a superimposed sketch of the first EW and SL wave functions (both for the electrons and heavy holes). We can see that introducing an enlarged well induces the formation of a localized state below the SL miniband. So the optically excited carriers, homogeneously created throughout the sample, move within the SL miniband as explained above and eventually reach the lower energy level of the enlarged well where they recombine. Therefore the EW luminescence is mainly due to the recombination of excitons photogenerated in

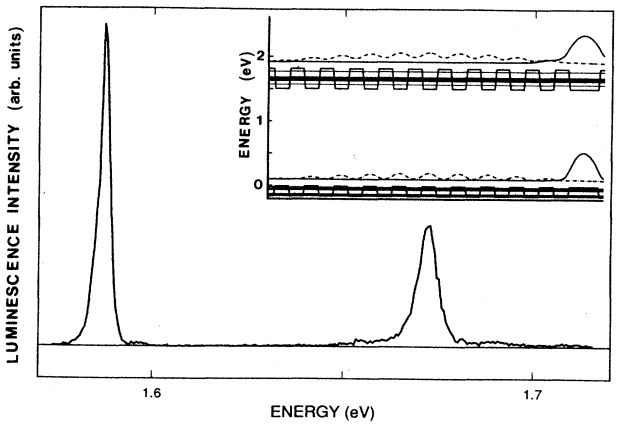

FIG. 4. Photoluminescence spectra at a bath temperature T of 4 K, of the 30 Å/30 Å ordered superlattice A. The excitation energy was of 1.718 eV and the excitation intensity was 130 mW cm^{-2}. The high-energy peak corresponds to luminescence from the superlattice (SL) and the low-energy peak is the emission associated with a single enlarged well (EW) of 60 Å grown in the superlattice. The inset shows a schematic diagram of the structure with the SL wells and barriers sequence (only 10 periods) and the enlarged well on the right. The SL minibands and the EW levels are plotted. Also sketched are the $n=1$ EW electronic and heavy-hole wave functions (solid lines) and the $n=1$ SL electronic and heavy-hole wave function (dashed lines) normalized to unity over the sample length. The zero of the energy scale is taken to be at the top of the GaAs valence band.

the superlattice. The contribution from excitons being directly photocreated in the EW is small because of the small optical density of the layer.

Let us define the ratio $R_L = L_{EW}/(L_{SL}+L_{EW})$, where L_{EW}, L_{SL} are the widths of the EW, and the superlattice, respectively. R_L is independent of the sample type ($R_L = 0.01$). We also define the ratio $R = I_{EW}/(I_{SPS}+I_{EW})$, where I_{EW}, I_{SPS} are the integrated emission intensities of the EW and the superlattice, respectively. According to the above model, R is bigger than R_L (for the spectrum shown in Fig. 4, R is equal to 0.7). Thus R is a measure of the number of excitons which move towards the enlarged well.

We show in Fig. 5 the photoluminescence spectra at 4 K of the purposely disordered sample B for different values of $\hbar\omega_x$. The spectrum shown in Fig. 5(a) was obtained with $\hbar\omega_x$ higher than the first electron and heavy-hole miniband edge. The four high-energy peaks [labeled SPS in Fig. 5(a)] at 1.692, 1.685, 1.670, and 1.652 eV are the excitonic superlattice emission associated with the different SL subbands. The low-energy peak (1.604 eV) is due to carrier recombination within the EW.[18]

In the ordered case, the ground-state SL (e-hh) excitons are formed between the electronic miniband and the first heavy-hole miniband. The energy separation is about 100 meV from the second excitonic miniband, thus we see a single-emission peak in the PL spectrum (Fig. 4). Heavy-hole excitons in a regular SL have been treated using a variational approach by Chomette *et al.*[19] For a 60-Å period superlattice, similar to the ordered sample A, they found a binding energy of about 5 meV, an excitonic Bohr radius in the layer plane of $\simeq 165$ Å, and an excitonic Bohr radius perpendicular to the layer of $\simeq 126$ Å (i.e., they found values very close to the GaAs bulk value of 146 Å). We can thus consider the excitons in our superlattices as quasi-three-dimensional.

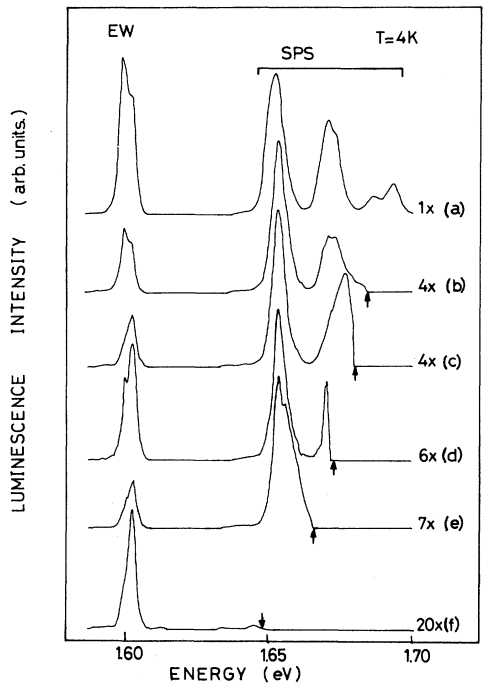

FIG. 5. Photoluminescence spectra of the disordered superlattice B at a bath temperature T of 4 K. The distribution of the well widths is 31 Å (19 times), 27 and 23 Å (8 times each), 35 Å (7 times), 39 Å (4 times), and 11, 15, and 19 Å once each, following a discrete Gaussian distribution. The corresponding emissions are labeled SPS. The emission line EW is due to a single 60 Å enlarged well grown in the superlattice. The excitation intensity was about 130 mW/cm^2. The excitation energies, indicated by arrows, are (a) 1.715, (b) 1.685, (c) 1.680, (d) 1.673, (e) 1.666, and (f) 1.648 eV. No luminescence was detected for energies above $\hbar\omega_x$. The relative sensitivity factors for the luminescence intensity are indicated on the right of the spectra.

In the disordered case, the excitons are formed between the wide electronic miniband and the heavy-hole subbands. The PL peaks observed are due to the recombination of excitons confined in different spatial regions and having different energies. The detailed structure of the SPS peaks cannot be reproduced with our calculations as we lack a model for the thermalization and recombination processes in a disordered SL. Despite this, we have tentatively assigned to each photoluminescence peak an excitonic transition involving a heavy-hole subband (see Table II). In the disordered case the transition rates are proportional to the spatial overlap between the involved wave functions (r selection rule).[20] To determine the transition energies E_t we have computed the overlap integrals between the wave functions of the heavy-hole states, with energy E_h belonging to a given subband, and all the electronic states, with energy E_e [E_h (E_e) is evaluated from the top (bottom) of the GaAs valence (conduction) band]. We have taken as E_t the energy $E_e+E_h+E_G-E_x$ of the first nonzero overlap integral, where E_G is the GaAs band-gap energy and $E_x = 5$ meV is the excitonic binding energy.[19] The computed values are shown in Table II. Our calculations yield five subbands, but we measure only four peaks in our photoluminescence spectra. The missing peak would occur at 1.638 eV. At that energy we observe a small feature in our spectra [see Fig. 5(a)]. But it remains an open problem why we do not observe a stronger recombination. It might be due to the low density of states connected with that transition.[21] As can be seen in Table II, we found a good agreement between the computed and measured transition energies at the 1.652 and 1.670 eV luminescence peaks whereas no agreement could be found for the higher-energy peaks. This can be due to the neglect of nonparabolicity and valence-band mixing in the calculation, an effect which is more relevant for thin wells.[22]

In Figs. 5(b)–5(f), the excitation energy decreases through the superlattice excitonic band. Comparing Fig. 4 with Fig. 5(a) we find, in the high-energy limit for $\hbar\omega_x$, that the ratio R is lower in the case of the disordered sample with respect to the ordered one. The R_L ratio is taken equal for both samples. This implies a reduction of exciton mobility due to disorder effects.[5] Figures 5(a) and 5(b) show that the number of excitons recombining in the EW depends also on $\hbar\omega_x$. We associate these variations with the optical excitation of extended or localized excitonic states. Let us now consider the motion in the vertical direction of a disordered SL. The eigenstates of

the stationary Schrödinger equation are localized (see Fig. 3). Therefore, propagation can occur by hopping between eigenstates localized in different spatial regions. If the exciting energy corresponds to an excitonic subband state formed by the superposition of extended electronic and confined heavy-hole wave functions, the exciton can propagate through a percolation motion and there is enhancement of recombination in the EW. Figure 5(d) illustrates this situation: The EW intensity increases and becomes comparable to that of the lowest-energy SPS peak. If the exciting energy corresponds to excitonic states at the subband extrema, where the wave functions are formed by electronic and heavy-hole localized states, the excitons are confined in definite wells within the SL. This reduces the luminescent emission from the EW [see Figs. 5(c) and 5(e)]. The number of excitons recombining in the EW decreases as the SL becomes transparent to the exciting light, and the only contribution left is that of the excitons created in the EW itself [Fig. 5(f)].

In Fig. 6 we plot the PL spectra of the disordered sample taken at different temperatures for a fixed $\hbar\omega_x$ (1.756 eV). When the temperature is increased, the high-energy part of the spectrum progressively disappears, and at about 70 K only the EW emission remains. This is in contrast with the expected behavior for uniform thermalization of excitons in a band. The population of the higher-energy states would be favored due to the increase of the mean kinetic excitonic energy. Consequently, an enhancement of the high-energy part of the photoluminescence spectrum would result. We interpret the quenching of the high-energy transitions as due to the detrapping of excitons from the localized states of the SL. Thus excitons can move to the EW where they recombine.

Moreover the spectral position of the luminescence peaks changes in energy as the temperature increases. There is a blue shift of the order of 2.5 meV when passing from 4 to 25 K. For higher T, the PL peaks decrease in energy due to the thermal reduction of the band gap. The initial blue shift of PL lines is due to the detrapping of localized excitons. The luminescence for $T \geq 25$ K is due to delocalized excitons whereas that for $T \leq 25$ K is due to localized excitons. Finally at 70 K, we have a complete thermalization and all the excitons recombine in the EW region.

A better demonstration of these facts is given in Fig. 7, where we report the ratio R as a function of $\hbar\omega_x$ for

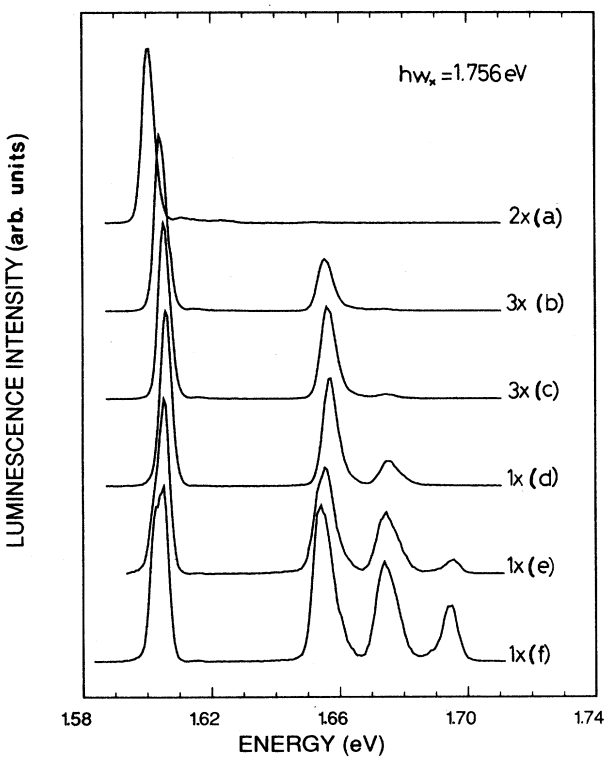

FIG. 6. Photoluminescence spectra of the disordered superlattice B at different sample temperatures T, respectively, (a) 70, (b) 50, (c) 40, (d) 20, (e) 10, and (f) 4 K. The excitation intensity was about 130 mW/cm^2 and the excitation energy $\hbar\omega_x$ was 1.756 eV. The relative sensitivity factors for the luminescence intensity are indicated at the right of the spectra. The decrease of the quantum efficiency as T increases is a well known fact and is due to the thermal activation of nonradiative recombination channels.

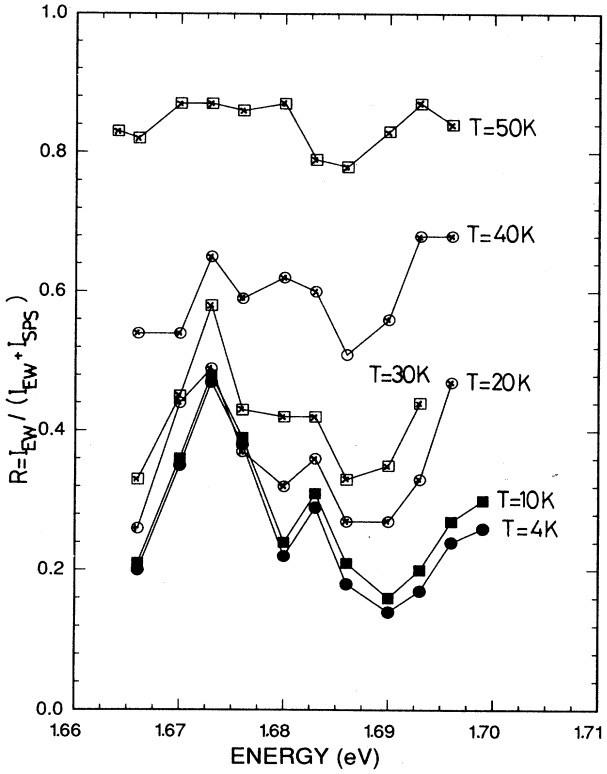

FIG. 7. The excitation energy dependence of R at the different sample temperatures indicated on the figure, for the disordered superlattice B. Where R is the ratio of the integrated emission from the enlarged well I_{EW} to the total integrated spectral emission $I_{EW}+I_{SPS}$ (where I_{SPS} is the integrated emission from the superlattices). The lines between the points are only a guide for the eyes.

different temperatures. For $T=4$ K the observed variation in R reflect the generation of alternatively mobile and localized excitons and cannot be explained by variations in the absorption coefficient.[6] The ratio R grows by increasing T which indicates an enhanced excitonic motion towards the EW. The minima in R also progressively disappear. Within the experimental errors R is quasi-independent of $\hbar\omega_x$ at 50 K. At $T=70$ K no luminescence is seen from the SL for any values of $\hbar\omega_x$, and R reaches the constant value of one. The increase in the mobility of excitons is due to phonon-assisted transition caused by the exciton-phonon interactions.

In Fig. 8 we show $\ln R$ versus $100/T$ for some $\hbar\omega_x$. These values of $\hbar\omega_x$ correspond to the excitation of localized excitons. For low T ($T \leq 20$ K) and energies $\hbar\omega_x$ belonging to subband edges, the excitonic states are localized. Propagation is expected to occur through variable range hopping between states of a given subband.[8] Energy separations for these states are of the order of 0.05 meV (see Table III). For a three-dimensional system, which is almost our case, this process has a characteristic T dependence of the form

$$\ln(\sigma) \simeq -\frac{B}{T^{0.25}} , \tag{3}$$

where σ is the system conductance.[8] According to our model, we have fitted the $\ln(R)$ versus T with a similar expression. The results are shown in Fig. 8 for a characteristic $\hbar\omega_x$, where the points are the experimental data and the dashed curve is the result obtained by fitting with Eq. (3). In Ref. 23 similar results were found by resonant Raman measurements on quantum wells. For intermediate temperatures ($T > 20$ K) we observe an activationlike behavior. We can fit the data with the $-E_A/k_BT$ law (solid curve in Fig. 8). Consequently, the characteristic energies for this regime are the energy separations between subbands (Table III). At higher temperatures, transfer toward the EW becomes more efficient and is by extended Bloch states.

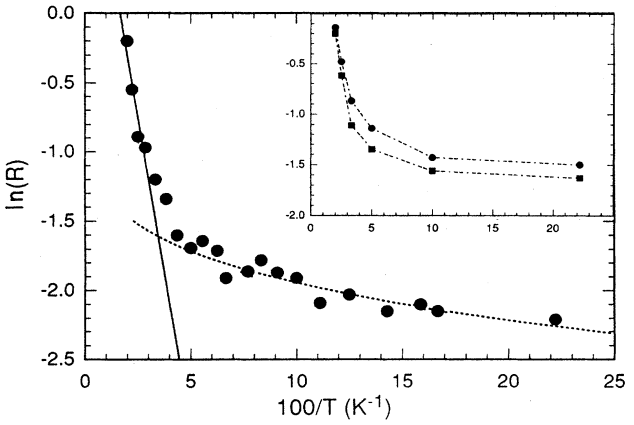

FIG. 8. Logarithm of the ratio R (see the caption to the Fig. 7 for a definition of R) vs the inverse of the sample temperature T. The experimental data were obtained by selective energy photoluminescence measurements on the disordered superlattice B. The excitation energy was 1.690 eV. The dotted curve is a fit to the data with Eq. (3) which is characteristic for variable range hopping. The continuous curve is a fit to the data in the intermediate temperature range with a linear relation characteristic for an activationlike behavior. The inset shows some experimental data for excitation energies of 1.680 eV (circle) and of 1.666 eV (square) which belong to different subbands. In this case the curves are only a guide for the eyes.

V. CONCLUSIONS

We have confirmed by using selective-excitation photoluminescence measurements that structural disorder in superlattices induces the formation of localized states. Studies of the integrated photoluminescence intensities as a function of $\hbar\omega_x$ show the existence of well-defined energy regions, where the excitons are more or less localized.

Simple calculations of the miniband stucture of the SL show widenings and splittings of SL minibands due to the random-layer sequence. The electron and heavy-hole wave functions are seen to be localized in this case. The miniband structure reflects itself in the excitation energy dependence of the photoluminescence spectra. We suggest that these effects are mainly due to the strong localization of the heavy-hole states.

From variable temperature SEPL we find indications for the existence of two temperature regimes for the vertical motion of excitons. The first regime corresponds to thermalization of excitons within the SL subbands by variable range hopping. The second regime indicates thermalization between the different excitonic subbands and is characterized by activation energies. Propagation towards EW is then by extended Bloch states.

More work, both experimental and theoretical, is needed to understand the details of our results. A calculation including excitonic effects is under way to explain the energy and temperature dependence of the excitonic motion.

TABLE III. Comparison between the experimental measured activation energies and some subband characteristic values. $\hbar\omega_x$ is the excitation energy. E_A is the average experimental activation energy obtained for different $\hbar\omega_x$ in the same subband. $\langle E \rangle$ is the mean energy in a heavy-hole subband. Δ/N is the energy separation between the eigenenergies in a subband. Δ_{gap} is the energy separation between the subband and the following.

$\hbar\omega_x$ (eV)	E_A (meV)	$\langle E \rangle$ (eV)	Δ/N (meV)	Δ_{gap} (meV)
		26	0.4	4
		31	0.2	6
1.666	4	36	0.056	6
1.680	6	42	0.014	9
1.690	5	51	0.011	

ACKNOWLEDGMENTS

We want to acknowledge D. Martin and F. Morier-Genoud for the growth of the sample, F. Lévy for kindly disposing some instrumentation, and M. A. Dupertuis, P. Von Allmen, and K. Maschke for fruitful discussions. This work was made possible by the support of the Swiss National Science Foundation, the Swiss Federal Postal Administration (GD-PTT), and by collaborating with Thomson CSF.

[1]N. Trivedi and N. W. Aschroft, Phys. Rev. B **35**, 6084 (1987).
[2]B. Sutherland and M. Kohmoto, Phys. Rev. B **36**, 5877 (1987).
[3]S. Das Sarma and X. C. Xie, Phys. Rev. B **37**, 1097 (1988).
[4]R. Merlin *et al.*, Phys. Rev. Lett. **55**, 1768 (1985); J. Todal *et al.*, *ibid.* **57**, 1157 (1986).
[5]A. Chomette, B. Deveaud, A. Regreny, and G. Bastard, Phys. Rev. Lett. **57**, 1464 (1986).
[6]E. Tuncel, L. Pavesi, D. Martin, and F. K. Reinhart, Phys. Rev. B **38**, 1597 (1988).
[7]B. Deveaud *et al.*, Phys. Rev. Lett. **58**, 2582 (1987).
[8]N. F. Mott and E. A. Davies, *Electronic Processes in Non-Crystalline Materials* (Clarendon, Oxford, 1979).
[9]See, for example, D. Calecki, J. F. Palmier, and A. Chomette, J. Phys. C **17**, 5017 (1984).
[10]B. Deveaud *et al.*, Solid State Commun. **57**, 885 (1986).
[11]F. Capasso, K. Mohammed, A. Y. Cho, R. Hull, and A. L. Hutchinson, Phys. Rev. Lett. **55**, 1152 (1985).
[12]We have used the continuity of the total current, i.e., $\chi(z)$ and $[1/m(z)][d\chi(z)/dz]$, as the boundary condition at each interface. Moreover, $\chi(z)$ vanishes at both the ends of the finite superlattice.
[13]D. Martin, E. Tuncel, F. Morier-Genoud, J. L. Staehli, and F. K. Reinhart, Helv. Phys. Acta **60**, 205 (1987).
[14]See, for example, J. A. Brum and G. Bastard, Superlatt. Microstruct. **3**, 51 (1987).
[15]P. Loscaux and R. Théodor, Analyse Numérique Matricielle Appliquée à l'Arte de l'Ingénieur (Masson, Paris, 1987), Chap. 10.
[16]For the calculation the band-gap discontinuity between GaAs and $Al_xGa_{1-x}As$ was considered as $1.247x$ (eV) and it was distributed between conduction-band offset and valence-band offset at a rate of 65% and 35%.
[17]L. Pavesi, E. Tuncel, G. Zumbach, and F. K. Reinhart, in Proceedings of the 19th International Conference on the Physics of Semiconductors, Warsaw, 1988 (in press).
[18]We note that the EW emission is formed by a doublet. The origin of this splitting is not yet understood, but it could not be ascribed to interface fluctuations because of its low-energy value (it is only 2.9 meV with respect to the expected 5 meV splitting due to half-monolayer fluctuations).
[19]A. Chomette *et al.*, Europhys. Lett. **4**, 461 (1987).
[20]I. Ingers, K. Maschke, and S. Proennecke, Phys. Rev. B **37**, 6105 (1988).
[21]Preliminary photoluminescence measurements on a disordered SL, with 220 periods and a random Gaussian distribution of wells with the same mean and standard deviation as sample *B*, reveal a peak at 1.638 eV. E. Tuncel *et al.* (unpublished result).
[22]C. Andreani and A. Pasquarello (private communication).
[23]J. E. Zucker, A. Pinczuk, D. S. Chemla, and A. C. Gossard, Phys. Rev. B **35**, 2892 (1987).